# Visually Resolving the Direct Z-Scheme Heterojunction in CdS@$ZnIn_2S_4$ Hollow Cubes for Photocatalytic Evolution of $H_2$ and $H_2O_2$ from Pure Water

*Erhuan Zhang, Qianhong Zhu, Junheng Huang, Jia Liu,* Guoqiang Tan, Chengjun Sun, Tao Li, Shan Liu, Yuemei Li, Hongzhi Wang, Xiaodong Wan, Zhenhai Wen, Fengtao Fan and Jiatao Zhang,* Katsuhiko Ariga*

Dr, E. H. Zhang, Dr, J. Liu, Prof. G. Q. Tan, S. Liu, Y. M. Li, H. Z. Wang, X. D. Wan, Prof. J. T. Zhang
School of Materials of Science & Engineering, Beijing Institute of Technology Beijing,100081, China
E-mail: zhangjt@bit.edu.cn; liujia86@bit.edu.cn.

Dr, E. H. Zhang, Dr. J. Liu, S. Liu, Y. M. Li, H. Z. Wang, X. D. Wan, Prof. J. T. Zhang
Beijing Key Laboratory of Construction-Tailorable Advanced Functional Materials and Green Applications, Experimental Center of Advanced Materials, School of Materials Science & Engineering, Beijing Institute of Technology, Beijing 100081, China.

Q. H. Zhu, Prof. F. T. Fan
State Key Laboratory of Catalysis, Dalian Institute of Chemical Physics, Chinese Academy of Sciences, Dalian National Laboratory for Clean Energy, Zhongshan Road 457, Dalian 116023, China.

Dr. C. J. Sun, Prof. T. Li
X-ray Science Division, Argonne National Laboratory, Argonne, Illinois 60439, USA.

Prof. T. Li
Department of Chemistry and Biochemistry, Northern Illinois University, DeKalb, Illinois 60115, USA.

Prof. Z. H. Wen, Dr. J. H. Huang
CAS Key Laboratory of Design and Assembly of Functional Nanostructures, Fujian Provincial Key Laboratory of Nanomaterials, Fujian Institute of Research on the Structure of Matter, Chinese Academy of Sciences, Fuzhou 350002, PR China.

Prof. K. Ariga
World Premier International (WPI) Research Center for Materials Nanoarchitectonics (MANA), National Institute for Materials Science (NIMS), Tsukuba, Ibaraki 305-0044, Japan.

**Keywords:** Photocatalysis; direct Z-scheme; surface photovoltage; hollow structures; interfaces

**Abstract:** The direct Z-scheme heterojunction has been recently emerging as an appealing architecture for photocatalysts design. Its efficiency depends on the interfacial and structural features of the photocatalysts, and can be favoured by the development in probing techniques that enable to directly demonstrate the interfacial charge transfer behaviours under light illumination. In this study, the two-dimensional $ZnIn_2S_4$ nanosheets are grown on the surface of CdS hollow cubes to construct the CdS@$ZnIn_2S_4$ hierarchical hollow photocatalysts with chemically bonded interface. The visualized measurements based on spatial-resolved surface photovoltage spectroscopy, combined with other spectroscopic and simulation investigations, clearly disclose that the CdS@$ZnIn_2S_4$ hollow cubes constitute a highly efficient direct Z-scheme system. This accounts for the stoichiometric generation of $H_2$ and $H_2O_2$ from pure water observed for the CdS@$ZnIn_2S_4$ sulfide-only photocatalysts under visible light irradiation with an apparent quantum efficiency of 2.43 % at 400 nm. The present work demonstrates an effective protocol to achieve comprehensive insights into the charge transfer route at semiconductor heterojunction, and offers a viable way for constructing efficient sulfide-only photocatalysts for driving water splitting reaction.

Artificial photosynthesis which converts solar energy into chemical fuels via a clean and sustainable manner presents a compelling avenue for addressing the worldwide energy and environmental issues.[1] Among the diverse protocols developed for improving the conversion efficiency of artificial photosynthesis, construction of the direct Z-scheme (recently also termed step-scheme) photocatalytic system involving an oxidation photocatalyst directly faced with a reduction photocatalyst featuring “step” charge-transfer route at heterojunction is particularly attractive.[2] This is because it allows wide light-absorption range, and at the same time can retain the strong redox ability of electrons/holes spatially separated on different active sites, driven by the unique internal electric field and band bending at the interface region which favour fast recombination of electrons in the conduction band (CB) of oxidation photocatalyst and the

holes in the valence band (VB) of reduction photocatalyst. In comparison with the conventional Z-scheme systems relying on the use of redox pair or solid-state electron mediators, direct Z-scheme photocatalysts could strongly suppress the backward reaction as well as the light-shielding effect.[2,3] In recent several years, there is an increasing surge in creating direct Z-scheme photocatalysts by combining various semiconductor pairs capable of forming a staggered band alignment. However, currently, most of the reported direct Z-scheme photocatalysts are only amenable to the half reactions. Taking photocatalytic water reduction as an example, the photogenerated electrons are exploited to produce $H_2$ under the condition that the photogenerated holes could be immediately consumed by the sacrificial agents.[4] In particular, the stoichiometric generation of $H_2$ and $H_2O_2$ from solar water splitting, which offers a compelling alternative to replace current energy-intensive $H_2O_2$ production process,[5] has not been realized by the Z-scheme architecture. To make the direct Z-scheme photocatalysts feasible for water splitting in pure water, aside from exploring new semiconductor combinations, the interfacial and structural features of the composite photocatalyst also require judicious design to facilitate efficient generation and utilization of the photogenerated charge carriers.

Another significant obstacle for developing direct Z-scheme photocatalysts is that the similar energy band configuration between Type II and Z-scheme heterojunctions poses a challenge for identifying the interfacial charge migration direction. The prevalent methods used to support the direct Z-scheme mechanism include free radical capture experiment, time-resolved spectroscopy measurement, density functional theory (DFT) calculation, in situ X-ray photoelectron spectroscopy (XPS) analysis, etc. These characterization means have offered profound insight into understanding the transport pathway of photoexcited carriers across the interface.[6] However, there still exists a demand of exploring new tools that can afford more straightforward evidences to unequivocally distinguish the Z-scheme from the Type II heterojunction. In the past few years, the remarkable advances in Kelvin probe force

microscopy-based spatially resolved surface photovoltage technique (hereafter abbreviated as SPVM) have opened up a new horizon in visualizing the localized charge separation at surfaces and interfaces of the photocatalysts.[7] It is envisioned that such technique may be applicable to image the accumulation of photoexcited electrons and holes at the two sides of a staggered-edge-positioned interface and therefore attain direct differentiation between the two inverse charge transfer processes.[3a]

Herein, we report an efficient direct Z-scheme photocatalyst constructed by growing two-dimensional (2D) $ZnIn_2S_4$ nanosheets on the surface of CdS hollow cubes (denoted as CdS@$ZnIn_2S_4$) with chemically bonded interfaces. The SPVM technique is exploited to visually demonstrate the Z-scheme charge transfer pathway at the heterojunction of two semiconductors, and the result is in good agreement with the DFT and transient absorption (TA) spectroscopy investigations. Beneficial from the favourable interfacial and structural characteristics, the CdS@$ZnIn_2S_4$ hollow cubes exclusively made of sulfide semiconductors can split pure water into $H_2$ and $H_2O_2$ with a stoichiometric ratio close to 1:1 and an apparent quantum efficiency (QE) of 2.43 % (at 400 nm) under visible light irradiation. Moreover, simultaneous evolution of $H_2$ and $O_2$ was observed when this direct Z-scheme photocatalyst was further modified with $IrO_2$ cocatalyst. These results are exceptional since it is commonly considered that the sulfide materials cannot viably split water due to their tendency to be self-oxidized by the photogenerated holes. We believe the present study can provide a valuable paradigm and boost the development in creation of efficient photocatalytic systems toward solar-to-fuel conversion.

**Figure 1A** illustrates the synthetic procedure of the CdS@$ZnIn_2S_4$ hollow cubes (details see **Figure S1** and the experimental section). The cubic AgCl crystals were used as the templating precursors (**Figure S2**), which were converted to hollow $Ag_2S$ cubes by the anion exchange between $Cl^-$ and $S^{2-}$ (the formation of the hollow cavity was attributable to the Kirkendall effect, **Figure S3**),[8] and then were topologically transformed to the hollow CdS cubes via the cation

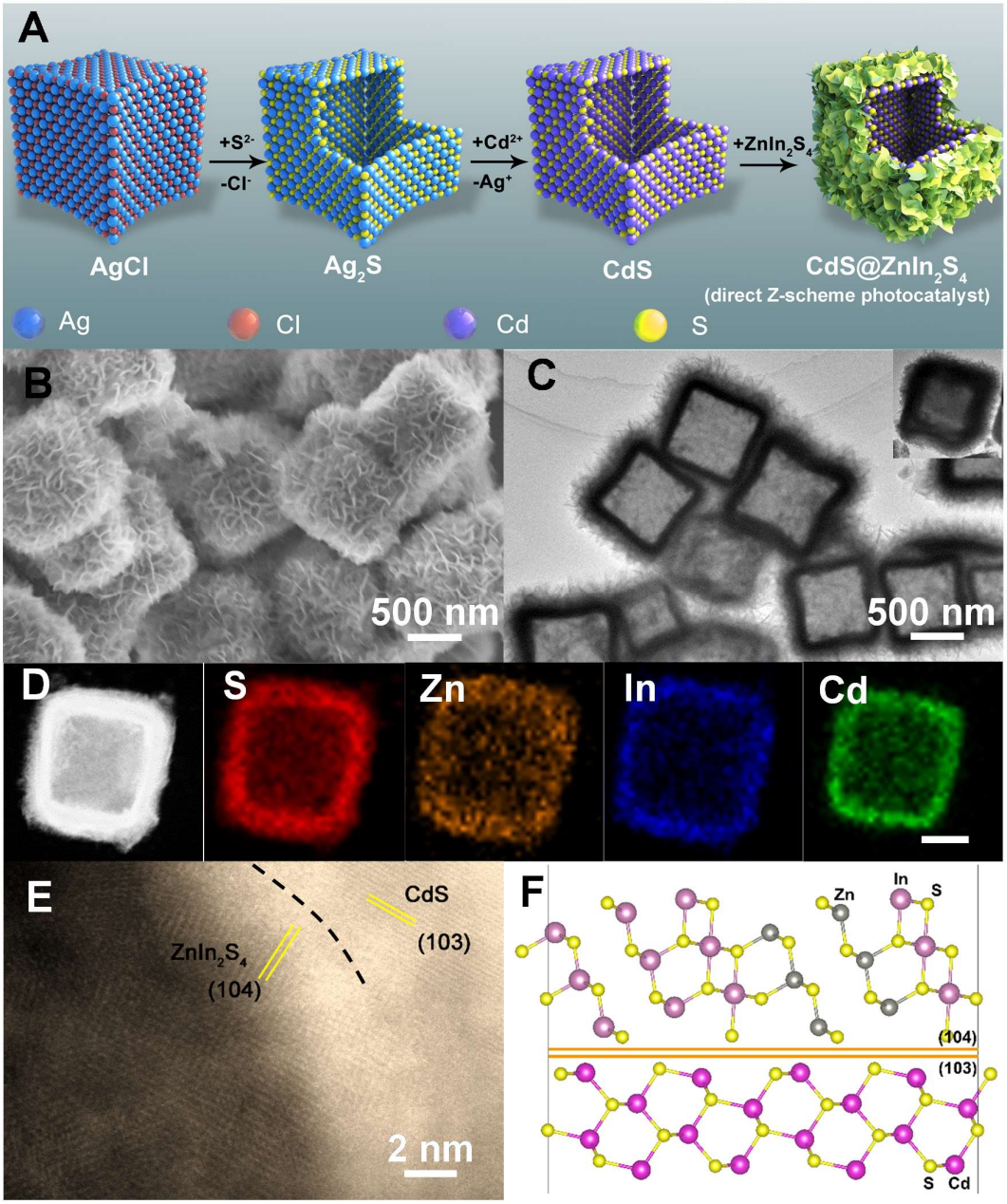


**Figure 1.** (A) Schematic illustration of the synthetic procedures for $CdS@ZnIn_2S_4$ hollow cubes (direct Z-scheme heterojunction). (B) FESEM image, (C) TEM image and (D) EDX elemental mapping results of $CdS@ZnIn_2S_4$ hollow cubes. (E) HRTEM image and the corresponding atomic model of the interface in $CdS@ZnIn_2S_4$ hollow cube.

exchange reaction between $Ag^+$ and $Cd^{2+}$ (**Figure S4**). Thereafter, the $ZnIn_2S_4$ nanosheets were in situ grown on the external surface of the yielded CdS cubes through a solvothermal process,

giving birth to the hierarchical CdS@$ZnIn_2S_4$ hollow cubes. The field emission scanning electron microscopy (FESEM) and transmission electron microscopy (TEM) images given in **Figures 1B**, **1C** and **S5** show that numerous nanosheets are densely assembled around each individual hollow cubes. The energy-dispersive X-ray spectroscopy (EDX) elemental mapping of a single hollow cube reveals that the S element is homogeneously distributed in the shell region, while the Zn and In elements are located on the periphery of the Cd element (**Figure 1D**), suggesting that the nanosheets wrapping around the CdS hollow cubes are composed by $ZnIn_2S_4$. This is further validated by the powder X-ray diffraction (XRD) pattern exhibited in **Figure S6**, which indicates the co-existence of hexagonal CdS (JCPDS NO. 41-1049) and hexagonal $ZnIn_2S_4$ (JCPDS No. 65-2023) in the final product. More importantly, the high-resolution TEM (HRTEM) image in **Figure 1E** discloses that the $ZnIn_2S_4$ nanosheets are directly grown on the CdS cubes, forming an intimate bonding between the (103) plane of CdS and the (104) plane of $ZnIn_2S_4$ at the interface (**Figure 1F**).

To establish a deeper view of the interfacial features of the CdS@$ZnIn_2S_4$ hollow cubes, the local atomic environments of Zn were investigated by analyzing the X-ray absorption near-edge structure (XANES) and extended X-ray absorption fine structure (EXAFS) spectra of the $ZnIn_2S_4$ nanosheets (**Figure S7**) before and after their growth on the surface of CdS hollow cubes (**Figure 2**). From **Figure 2A**, a slight shift in the near-edge absorption energy of CdS@$ZnIn_2S_4$ hollow cubes compared to $ZnIn_2S_4$ nanosheets can be noticed, which implies that growing on CdS surfaces might cause some impact on the chemical-bonding nature of the $ZnIn_2S_4$ components. To acquire quantitative structural parameters around the Zn atoms, we further performed the EXAFS measurements at the Zn K-edge. The results are given in **Figure 2B**, in which the R-space EXAFS spectrum for $ZnIn_2S_4$ nanosheets exhibited a dominant Zn-S coordination at 1.87 Å, while the Zn-S peak of CdS@$ZnIn_2S_4$ shifted to the high R direction (1.90 Å) with obviously decreased intensity, indicative of the changed local atomic arrangement

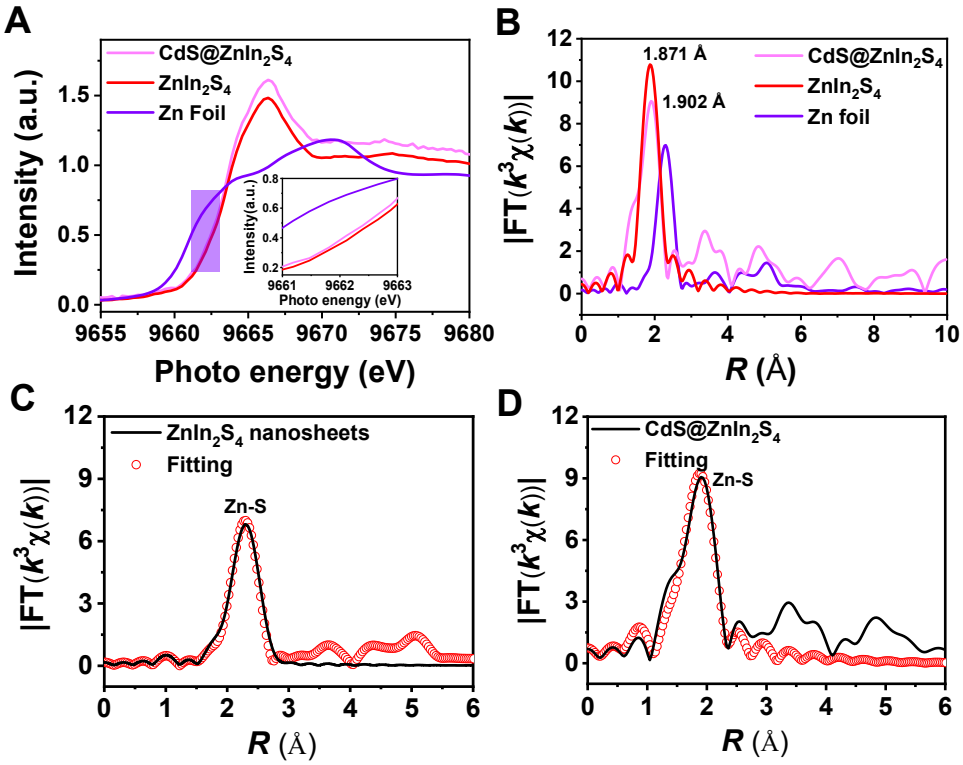


**Figure 2**. (A) Zn K-edge XANES spectra of $ZnIn_2S_4$ nanosheets and CdS@$ZnIn_2S_4$ hollow cubes (inset: the enlarged image of the region marked by purple). (B) $k^3$-weighted Fourier transform (FT) χ(k) function of the EXAFS spectra for $ZnIn_2S_4$ nanosheets and CdS@$ZnIn_2S_4$ hollow cubes. (C), (D) The corresponding EXAFS fitting curves of $ZnIn_2S_4$ nanosheets (C) and CdS@$ZnIn_2S_4$ (D) in R space.

of Zn and the strong interfacial interactions between CdS and $ZnIn_2S_4$ in CdS@$ZnIn_2S_4$.[9] Furthermore, the Zn-S coordination numbers were extracted from the EXAFS least-squares curve fitting (**Figures 2C**, **2D**, and **S8**). The coordination number of Zn-S was estimated to be 3.9 for $ZnIn_2S_4$ nanosheets but increased considerably to 5.1 for CdS@$ZnIn_2S_4$ hollow cubes (fitting parameters see **Figure S8**). Such findings unravel the existence of chemical bonding between CdS and $ZnIn_2S_4$ at the interface through bonding of Zn atoms in $ZnIn_2S_4$ with S atoms in CdS.[9a]

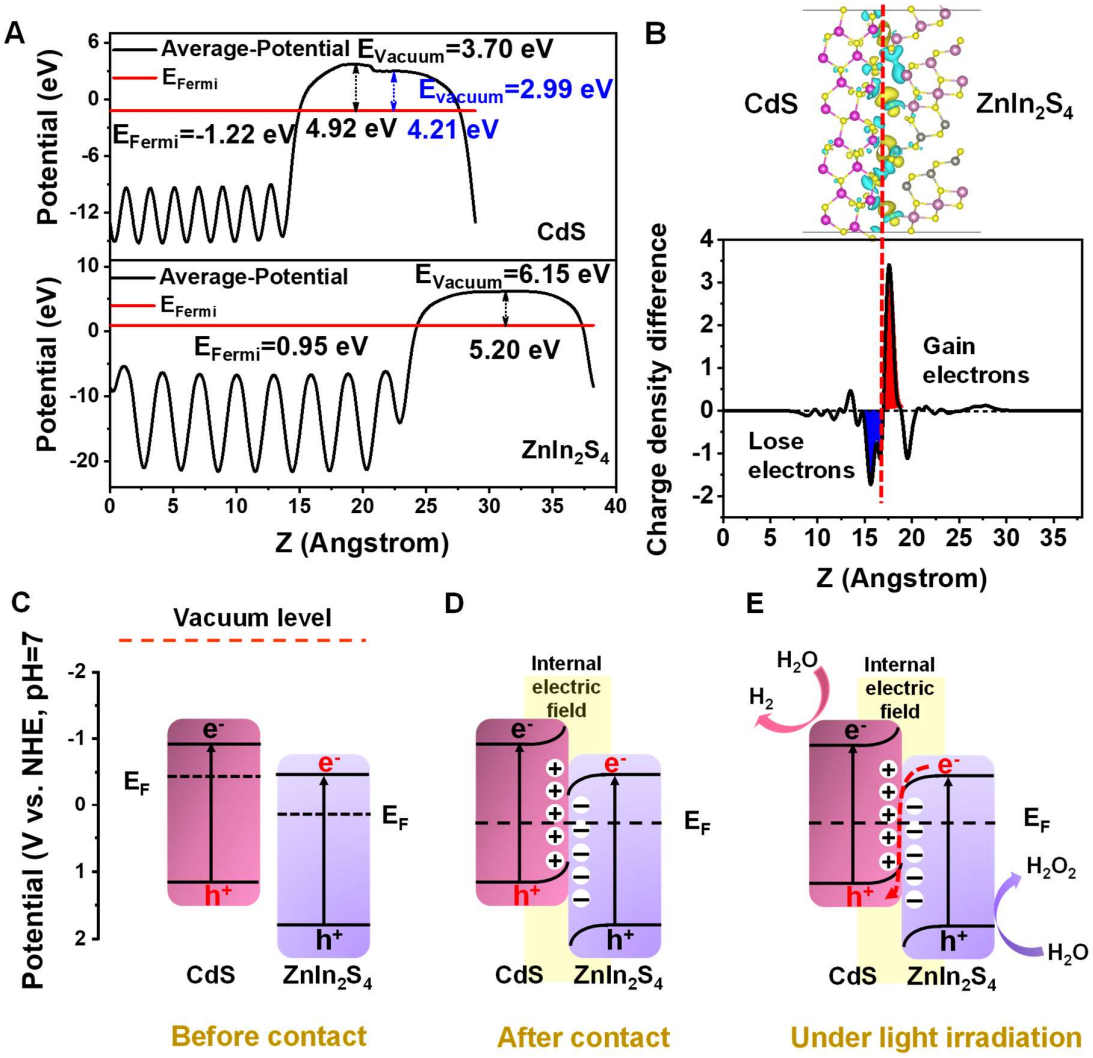


**Figure 3.** (A) Electrostatic potentials for the CdS (103) surface and the $ZnIn_2S_4$ (104) surface. (B) Simulated charge distributions at the interface of CdS-$ZnIn_2S_4$ when the Fermi level equilibrium is achieved. (C-E) Schematic diagram showing the energy band structure and the interfacial charge transfer for CdS@$ZnIn_2S_4$ hollow cubes: (C) before contact, (D) after contact, and (E) photogenerated charge transfer process in Z-scheme mode.

The Mott-Schottky plots suggested that the flat-band potentials (≈CB positions for n-type semiconductors) of CdS hollow cubes and $ZnIn_2S_4$ nanosheets were located around -0.90 and -0.57 V versus the normal hydrogen electrode (NHE, pH = 7), respectively (**Figure S9**). The

band gaps were estimated to be 2.21 and 2.53 eV for CdS and $ZnIn_2S_4$ correspondingly based on the Tauc plots shown in **Figure S10**. Therefore, the VB positions of CdS and $ZnIn_2S_4$ were calculated to be 1.31 and 1.96 V versus NHE (pH = 7), respectively. These results manifest the possibility of establishing a direct Z-scheme heterojunction in CdS@$ZnIn_2S_4$ hollow cubes that satisfies the thermodynamic requirement for water splitting.

First, the DFT calculations were conducted to predict the band bending at the formed CdS-$ZnIn_2S_4$ interface. As shown in **Figure 3A**, the work function of CdS (103) surface was estimated to be 4.92 and 4.21 eV, obviously smaller than that of the $ZnIn_2S_4$ (104) surface at 5.20 eV (**Figure 3C**). Therefore, upon the formation of a heterojunction between CdS (103) surface and $ZnIn_2S_4$ (104) surface, the electrons are prone to migrate from the CdS (103) surface having a higher Fermi level (-4.92 and -4.21 eV) to the $ZnIn_2S_4$ (104) surface with a lower Fermi level (-5.20 eV) to equilibrate the Fermi levels of the two components (**Figure S11**).[10] **Figure 3B** presents the simulated charge distribution profile and the corresponding 3D charge density difference plot of CdS-$ZnIn_2S_4$ interface when the Fermi level equilibrium is achieved, which signifies the appearance of an electron depletion layer in CdS and accumulation layer in $ZnIn_2S_4$ forming an internal electric field orientated from CdS to $ZnIn_2S_4$ (**Figure 3D**). As such, the photogenerated electrons in $ZnIn_2S_4$ incline to recombine with the photogenerated holes in CdS following the Z-scheme charge transfer path (**Figure 3E**).[11] This is consistent with the results of X-ray photoelectron spectroscopy (XPS) characterizations as presented in **Figure S12**. It can be seen that the characteristic peak of Cd 3d in CdS@$ZnIn_2S_4$ shifted to a higher binding energy (by 0.1 eV) relative to the CdS hollow cubes, whereas the binding energies of Zn 2p and In 3d in the composites displayed a negative shift (by 0.4 and 0.2 eV, respectively) in comparison with the $ZnIn_2S_4$ nanosheets. Such shifted binding energies in XPS spectra suggest an electron flow from CdS to $ZnIn_2S_4$ in the ground electronic state,[6d,12] which can be justified by the formation of interfacial band bendings that favour the direct Z-scheme mechanism.

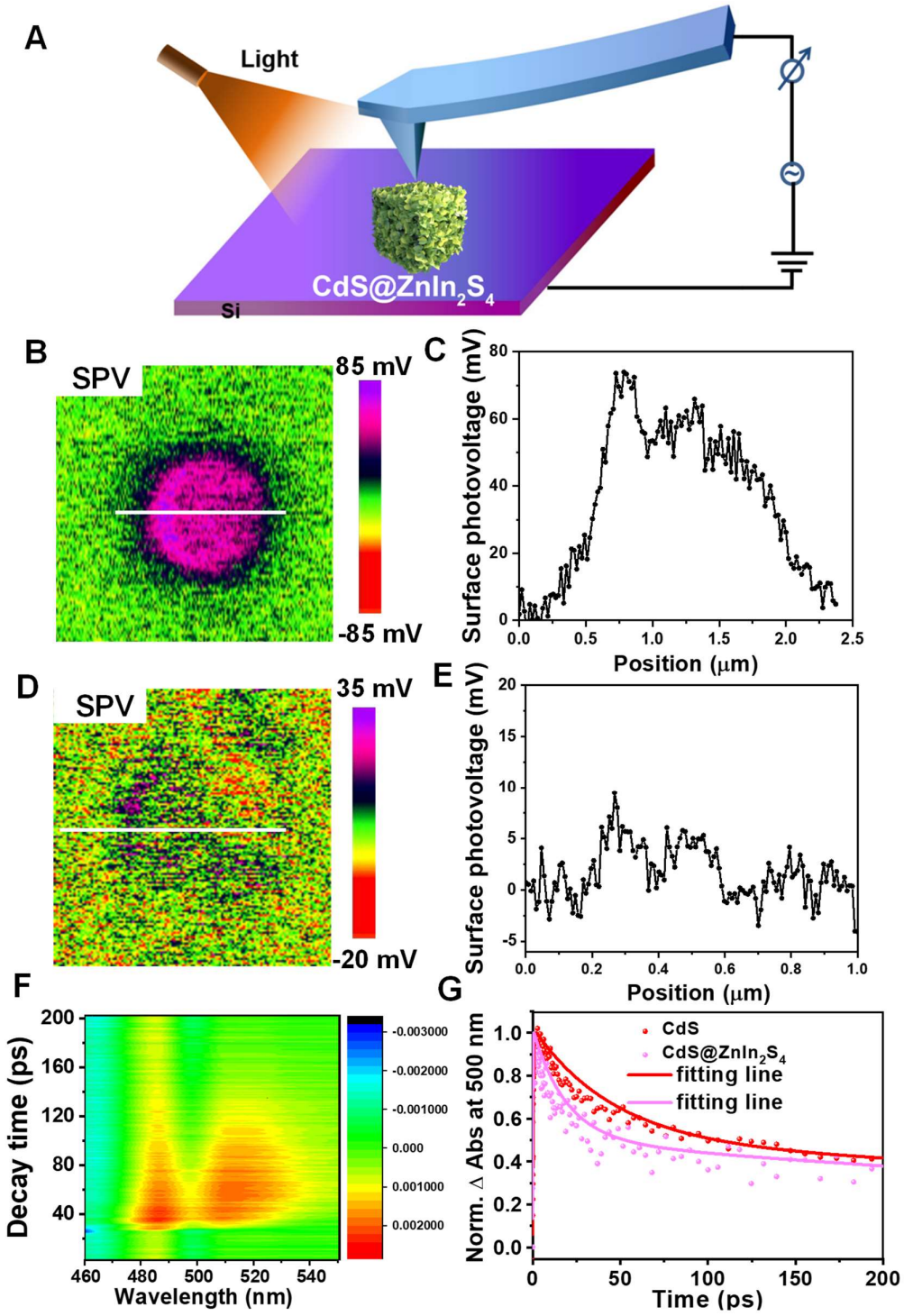


**Figure 4.** (A) Experimental set-up for SPVM imaging of $CdS@ZnIn_2S_4$ hollow cubes. (B) SPV mapping image of a $CdS@ZnIn_2S_4$ hollow cube excited with 450 nm light and (C) the corresponding SPV signal measured along the white line denoted in Figure (B). (D) SPV mapping image of a CdS hollow cube excited with 450 nm light and (E) the corresponding SPV signal measured along the white line denoted in the Figure (D). (F) 2D pseudo-color plot of TA

spectra for CdS@$ZnIn_2S_4$ hollow cubes at 400 nm excitation. (G) Normalized TA profiles probed at 500 nm for the CdS hollow cubes (red) and CdS@$ZnIn_2S_4$ (pink) under 400 nm excitation.

Importantly, as aforementioned, to promote the development of direct Z-scheme photocatalysts, it is imperative to explore new techniques that can realize more direct determination on the charge-carrier migration pathway across the staggered heterojunction under light irradiation. To this end, in this study the SPVM was adopted to give the visualized demonstration on the direct Z-scheme mechanism. This is based on the high reliability of the SPVM technique in simultaneously imaging the surface morphology and the photo-induced changes in surface potential over the photocatalyst with a high spatial resolution (nano-meter scale) and high potential sensitivity (mV).[7] The set-up of the SPVM is schematically illustrated in **Figure 4A**. The topography (**Figure S13A**) and surface potentials of the sample were measured using a Pt/Ir-coated tip (SCM-PIT, Bruker) grounded to the substrate under ambient conditions. **Figures S13B** and **S13C** present the corresponding surface potential images of a single CdS@$ZnIn_2S_4$ particle under dark and illumination ($\lambda$ = 450 nm) conditions, respectively. To clearly contrast the alterations in surface potential caused by light illumination, the surface photovoltage (SPV) mapping image for CdS@$ZnIn_2S_4$ was acquired by subtracting the illuminated surface potential image from that in the dark. From **Figure 4B**, one can observe that the SPV image of CdS@$ZnIn_2S_4$ exhibits a dramatic positive change as large as 73 mV upon light illumination (**Figure 4C**). Such variation of SPV signal is much more significant than that of the CdS hollow cubes under the same measurement conditions (**Figures 4D**, **4E** and **S14**), implying the existence of a built-in electric field in CdS@$ZnIn_2S_4$ that is stronger than or competitive with those caused by cocatalyst loading, phase junction and crystal facet architecture.[7c,13] As the $ZnIn_2S_4$ nanosheets formed a thick coating layer around the CdS hollow cubes in the CdS@$ZnIn_2S_4$ composites (i.e. the CdS component was impossible to be

probed by the tip, **Figure 1** and **S5**), the positive SPV signal measured for CdS@$ZnIn_2S_4$ can be exclusively assigned to the surface potential change of $ZnIn_2S_4$. The results vividly manifest the accumulation of photogenerated holes in the region of $ZnIn_2S_4$ nanosheets when the two components of CdS@$ZnIn_2S_4$ are concurrently excited, which unambiguously reveals the photo-induced vectorial electron transfer from $ZnIn_2S_4$ to CdS. This complies with the direct Z-scheme pathway as depicted in **Figure 3E**, strongly corroborating the inference derived from DFT calculation and XPS characterization discussed previously.

In addition, the femtosecond time-resolved TA spectroscopic measurements were performed under 400 nm excitation to further probe the dynamics of photogenerated charge carriers in CdS@$ZnIn_2S_4$ hollow cubes. It has been reported that the peaks in the range of 400-700 nm in TA spectra are generally attributed to the surface-trapped holes.[6c,14] Therefore, we consider that the notable absorption bands around 480-540 nm observed for CdS@$ZnIn_2S_4$ (**Figure 4F**) and CdS hollow cubes (**Figure S15**) after excitation are characteristic of the trapped holes. **Figure 4G** exhibits the TA decay profiles of the two samples probed at 500 nm, which can be both fitted by a two-exponential function. In virtue of the fast charge recombination rate in pure $ZnIn_2S_4$ nanosheets (**Figure S16**) and the main content (64 wt%, **Figure S17**) of CdS in CdS@$ZnIn_2S_4$ composites, the TA signal detected for CdS@$ZnIn_2S_4$ hollow cubes should be principally contributed by the excited CdS.[6c,15] In comparison with the pure CdS hollow cubes ($\tau_1$ = 47.5 ± 4.3 ps and $\tau_2$ = 1143.8 ±110 ps), the decay lifetimes of CdS@$ZnIn_2S_4$ are substantially reduced ($\tau_1$= 19.5 ±3.7 ps and $\tau_2$ = 667.3 ±125 ps). Similar phenomena have been reported in previous studies and rationalized by the migration of photogenerated holes from the VB of reduction photocatalyst (CdS in our case) to the CB of oxidation photocatalyst ($ZnIn_2S_4$ in our case) in accordance with the Z-scheme pathway.[6c,9a,15]

The consistent results of above characterizations afford consolidate proofs that the CdS@$ZnIn_2S_4$ hollow cubes constitute a valid direct Z-scheme photocatalytic system. The performance of the samples in photocatalytic water splitting was measured under visible light

irradiation ($\lambda > 400$ nm) without using any sacrificial agents. As exhibited in **Figure 5A**, in pure water, the CdS hollow cubes and $ZnIn_2S_4$ nanosheets showed no and negligible $H_2$ evolution activities, respectively (details see **Figure S19**). However, in sharp contrast, the CdS@$ZnIn_2S_4$ hollow cubes displayed a remarkable $H_2$ evolution rate of 540.3 μmol $g^{-1}$ $h^{-1}$ under the same conditions. This is 3 orders of magnitude enhanced relative to the physical mixture of CdS hollow cubes and $ZnIn_2S_4$ nanosheets (0.2 μmol $g^{-1}$ $h^{-1}$, **Figure S20**), clearly disclosing the significant role of the chemically bonded interface between CdS and $ZnIn_2S_4$ for achieving efficient charge transfer at the heterojunction. The photoluminescence (PL) spectra, photoelectrochemical (PEC) currents and electrochemical impedance spectroscopy (EIS) plots were also compared for the different samples (**Figure S21**), which additionally support the enhanced utilization of photogenerated carriers enacted by the construction of CdS@$ZnIn_2S_4$ Z-scheme heterojunction. According to **Figure 5B**, there was no significant decay in $H_2$ evolution rate for CdS@$ZnIn_2S_4$ hollow cubes during four consecutive cycles. This is in good agreement with the TEM, FESEM, XRD and XPS measurements given in **Figures S22** and **S23**, suggesting subtle photocorrosion occurred to the sulfide samples under accumulative visible light irradiation for 12 h in pure water. It has long been thought that the sulfide semiconductors cannot be explored as stable photocatalysts without the assistance of hole sacrificial agents. However, very recently, Xiong and Chen respectively demonstrated that by constructing Janus-like structure or doping with heteroatoms, the pure sulfide materials were capable of evolving $H_2$ in the absence of sacrificial agents, albeit the activities were modest and the ratio between $H_2$ and the oxidative products ($O_2$ or $H_2O_2$) was non-stoichiometric.[4a,16] The remarkable results in our study further underpin the importance of elaborately engineering the interfacial and structural properties of the sulfide-based photocatalysts for fully harnessing their great potential toward artificial photosynthesis.

It should be noted that no $O_2$ gases were detected during the whole reaction process, suggesting there were other water oxidation intermediates or products. As shown in Figure 5C,

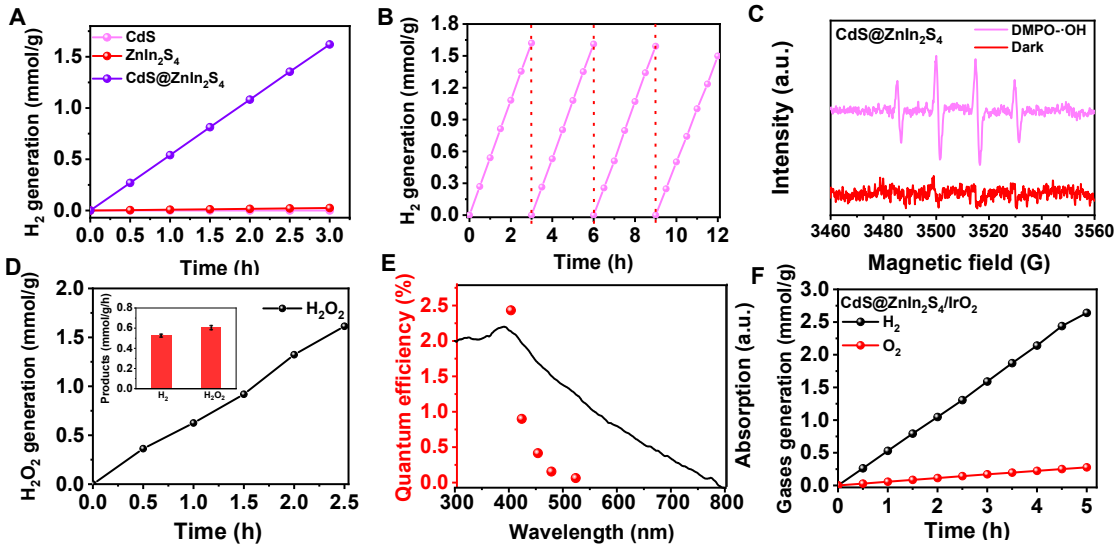


**Figure 5.** (A) Time courses of $H_2$ evolution for different samples in pure water under > 400 nm light irradiation. (B) Recycling performance of CdS@$ZnIn_2S_4$ hollow cubes in photocatalytic pure water splitting. (C) ESR signals of the DMPO-•OH spin adducts in CdS@$ZnIn_2S_4$ aqueous suspension under light irradiation and dark conditions, respectively. (D) Time course of $H_2O_2$ production for CdS@$ZnIn_2S_4$ hollow cubes in pure water under > 400 nm light irradiation (inset: the ratio of evolved $H_2$ and $H_2O_2$ close to 1:1). (E) Wavelength-dependence of AQE for CdS@$ZnIn_2S_4$ hollow cubes in photocatalytic pure water splitting. (F) Time courses of $H_2$ and $O_2$ evolution for CdS@$ZnIn_2S_4$/$IrO_2$ (CdS@$ZnIn_2S_4$ hollow cubes tailored with 1.5 wt% $IrO_2$ cocatalysts) in pure water under > 400 nm light irradiation.

under light irradiation, four characteristic signals of DMPO-•OH with an intensity ratio of 1:2:2:1 appeared in the electron spin resonance (ESR) spectrum for the CdS@$ZnIn_2S_4$ aqueous suspension, indicative of the generation of hydroxyl radicals (•OH) in accompany with the photocatalytic $H_2$ evolution from water. Considering that the redox potential of •OH/$H_2O$ was reported around 1.6 ~ 1.9 V vs NHE (pH = 7),[17] while the VB edges of CdS and $ZnIn_2S_4$ are

located at 1.31 and 1.96 V vs NHE (pH = 7), correspondingly (**Figure 3C**), the successful detection of •OH species further authenticated the Z-scheme charge transfer mechanism. Even remarkably, a substantial amount of $H_2O_2$ was detected, which increased linearly with the proceeding of the photocatalytic reaction (**Figures 5D** and **S24**). The $H_2O_2$ evolution rate was determined to be 604.8 μmol $g^{-1}$ $h^{-1}$, comparable to the $H_2$ evolution rate with a stoichiometric ratio close to 1:1 (inset of **Figure 5D**). On these bases, we propose that the CdS@$ZnIn_2S_4$ hollow cubes are capable to drive one- and/or two-electron water oxidation involving the formation of •OH and $H_2O_2$ as oxidation species.[18] The apparent quantum efficiency (AQE) of $H_2$ production was also measured for CdS@$ZnIn_2S_4$ as a function of the incident light wavelength without using any sacrificial agents and cocatalysts (**Figure 5E**). A considerable value of 2.43 % was achieved at λ = 400 nm, indicating the superior activity of CdS@$ZnIn_2S_4$ in photocatalytic pure water splitting. Besides, very interestingly, simultaneous $H_2$ and $O_2$ evolution was observed when the CdS@$ZnIn_2S_4$ hollow cubes were further tailored with 1.5 wt% $IrO_2$ cocatalysts (denoted as CdS@$ZnIn_2S_4$/$IrO_2$, **Figures 5F** and **S25**).

By virtue of comprehensive theoretical calculation, Nøvskov et al. proposed that ΔGO $\gtrsim$ 3.5 eV (where ΔGO refers to the free energy of O*, a critical intermediate in water oxidation process) is a criterion that leads the product selectivity toward $H_2O_2$ instead of $O_2$ in water oxidation reaction.[19] In our study, the high efficiency for $H_2O_2$ generation observed for the CdS@$ZnIn_2S_4$ hollow cubes might be associated with a suitable free energy of the O* species adsorbed on the surface of $ZnIn_2S_4$ nanosheets. On the other hand, $IrO_2$ is known both experimentally and theoretically to be the excellent catalysts for $O_2$ evolution as a result of the small free energy of adsorbed O* (ΔGO far below 3.5 eV).[19] Therefore, the presence of $O_2$ in water splitting reaction over CdS@$ZnIn_2S_4$/$IrO_2$ was probably owing to the strong driving force of the $IrO_2$ cocatalysts for complete four-electron oxidation. The non-stoichiometric ratio of the evolved $H_2$ and $O_2$ gases could be explained by the possibility that the water oxidation reaction

also occurred on the surface of $ZnIn_2S_4$ nanosheets aside from $IrO_2$. More significantly, it should be pointed out that the excellent performance of CdS@$ZnIn_2S_4$ hollow cubes in photocatalytic pure water splitting was very likely originated from their prominent structural and interfacial properties. For example, the hollow cavity of the CdS cubes are beneficial for light harvesting due to the light scattering effect (**Figure S26**);[4b,20] the 2D nature of $ZnIn_2S_4$ nanosheets permits short migration path for carriers to reach surface and the abundant surface reactive sites;[6c,9b,15,21] the chemically bonded CdS-$ZnIn_2S_4$ heterojunction with favourable internal electric field could accelerate the recombination of undesirable photogenerated carriers at the interface,[9a,22] and therefore preserve the valuable electrons at the CB of CdS and holes at the VB of $ZnIn_2S_4$ to make them efficiently participate in the reaction.

In conclusion, the CdS@$ZnIn_2S_4$ hollow cubes with well-defined hetero-interfaces were fabricated, which showed exceptional performance in photocatalytic pure water splitting. The nanoscopically-resolved SPVM technique was exploited to give the first visualized demonstration on the formation of the direct Z-scheme heterojunction between CdS and $ZnIn_2S_4$ in CdS@$ZnIn_2S_4$, and the conclusion was further supported by a series of simulation and spectroscopic investigations. Without using any sacrificial agents or cocatalysts, stoichiometric $H_2$ and $H_2O_2$ were detected from pure water under visible light irradiation in the presence of CdS@$ZnIn_2S_4$ photocatalysts that were solely composed of sulfide semiconductors. Such remarkable photocatalytic ability of CdS@$ZnIn_2S_4$ could be justified by their structural and interfacial properties which are in favour of fast interfacial charge transfer via the Z-scheme pathway. Our findings underline the important principles for constructing the Z-scheme architecture from the aspect of structural/interfacial design, which can also be applicable for creating stable sulfide photocatalysts, and exemplify the great potential of the SPVM technique for distinguishing the confusable charge migration pathway at the staggered heterojunction in photocatalysts.

**Supporting Information**
Supporting Information is available from the Wiley Online Library or from the author.

**Acknowledgements**
This work was supported by the National Natural Science Foundation of China (Grant No. 51702016, 51631001, 21801015, 51902023, 51872030), the Fundamental Research Funds for the Central Universities 2017CX01003 and the Beijing Institute of Technology Research Fund Program for Young Scholars. We thank Prof. Can Li in Dalian Institute of Chemical Physics, Chinese Academy of Sciences, for his kind support in SPVM characterization. Use of the Advanced Photon Source (APS, 20-BM beamline), Office of Science user facilities, was supported by the U. S. Department of Energy (DOE), Office of Science, Office of Basic Energy Sciences, under Contract No. DE-AC02-06CH11357. The authors acknowledge the critical testing work supported by Beijing Zhongkebaice Technology Service Co., Ltd.

Received: ((will be filled in by the editorial staff))
Revised: ((will be filled in by the editorial staff))
Published online: ((will be filled in by the editorial staff))

**References**

[1] a) J. Esswein, D. Nocera, *Chem. Rev.* **2007**, *107*, 4022; b) Q. Wang, K. Domen, Chem. Rev. **2019**, *120*, 919-985; c) H. Abe, J. Liu, K. Ariga. *Mater. Today* **2016**, 19, 12; d) D. Walsh, N. Sanchez-Ballester, K. Ariga, A. Tanaka, Mark Weller, *Green Chem*. **2015**, 17, 982; e) L. Hammarström, S. Hammes-Schiffer, *Acc. Chem. Res*. **2009**, *42*,1859.

[2] a) Q. Xu, L. Zhang, B. Cheng, J. Fan, J. Yu, Chem 2020, *6*,1543-1559; b) H. Li, W. Tu, Y. Zhou, Z. Zou, *Adv. Sci*. **2016**, *3*, 1500389; c) J. Low, C. Jiang, B. Cheng, S. Wageh, A. Al-Ghamdi, J. Yu, Small Methods **2017**, *1*, 1700080; d) F. Xu, K. Meng, B. Cheng, S. Wang, J. Xu, J. Yu, Nat. Commun. **2020**, *11*, 4613.

[3] Y. Wang, H. Suzuki, J. Xie, O. Tomita, D. Martin, M. Higashi, D. Kong, R. Abe, J. Tang, Chem. Rev. **2018**, *118*, 5201; b) P. Zhou, J. Yu, M. Jaroniec, Adv. Mater. **2014**, *26*, 4920; c) Y. Qi, Y. Zhao, Y. Gao, D. Li, Z. Li, F. Zhang, C. Li, Joule **2018,** *2*, 2393.

[4] a) Q. Yuan, D. Liu, N. Zhang, W. Ye, H. Ju, L. Shi, R. Long, J. Zhu, Y. Xiong, Angew. Chem. Int. Ed. **2017**, 56, 4206; b) B. Qiu, Q. Zhu, M. Du, L. Fan, M. Xing, J. Zhang, *Angew. Chem. Int. Ed.,* **2017**, *56*, 2684.

[5] a) W. Fan, B. Zhang, X. Wang, W. Ma, D., Li, Z. Wang, M. Dupuis, J. Shi, S. Liao, Li. C, *Energy Environ. Sci.* **2020**, 13, 238; b) Y. Kofuji, Y. Isobe, Y. Shiraishi, H. Sakamoto, S. Tanaka, S. Ichikawa, T. Hirai, *J. Am. Chem. Soc.* **2016**, *138*, 10019; c) K. Ariga, X. Jia, J. Song, J. P. Hill, D. T. Leong, Y. Jia, J. Li, *Angew. Chem. Int. Ed.* **2020**, *59*, 15424; d) J. Liu, H. Zhou, W. Yang, K. Ariga, *Acc. Chem. Res.* **2020**, *53*, 644.

[6] a) Z. Zhang, J. Huang, Y. Fang, M. Zhang, K. Liu, B. Dong, *Adv. Mater*. **2017**, *29*, 1606688; b) X. She, J. Wu, H. Xu, J. Zhong, Y. Wang, Y. Song, K. Nie, Y. Liu, Y. Yang, M. Rodrigues, R. Vajtai, J. Lou, D. Du, H. Li, P. Ajayan, *Adv. Energy Mater*. **2017**, *7*, 1700025; c) M. S. Zhu, Z. C. Sun, M. Fujitsuka, T. Majima, *Angew. Chem. Int. Ed*. **2018**, *130*, 2182; d) Q. Xu, B. Zhu, C. Jiang, B. Cheng, J. Yu, *Sol. RRL* **2018**, *2*, 1800006; e) J. X. Low, B. Z. Dai, T. Tong, C. J. Jiang, J. G. Yu, *Adv. Mater*. **2018**, *31*, 1802981.

[7] a) J. Zhu, F. Fan, R. Chen, H. An, Z. Feng, C. Li, *Angew. Chem. Int. Ed*. **2015**, *54*, 9111; b) H. Li, Y. Gao, Y. Zhou, F. Fan, Q. Han, Q. Xu, X. Wang, M. Xiao, C. Li, Z. Zou, *Nano Lett*. **2016**, *16*, 5547; c) J. Zhu, S. Pang, T. Dittrich, Y. Gao, W. Nie, J. Gui, R. Chen, H. An, F. Fan, C. Li, *Nano Lett*. **2017**, *17*, 6735; d) R. Chen, F. Fan, T. Dittrich, C. Li, *Chem. Soc. Rev*. **2018**, *47*, 8238; e) R. Chen, S. Pang, H. An, J. Zhu, S. Ye, Y. Gao, F. Fan, C. Li, *Nat. Energy* **2018**, *3*, 655.

[8] Q. Kuang, S. Yang, *CrystEngComm* **2014**, *16*, 4940.

[9] a) P. Wang, Y. Mao, L. Li, Z. Shen, X. Luo, K. Wu, P. An, H. Wang, L. Su, Y. Li, S. Zhan, *Angew. Chem. Int. Ed.,* **2019**, *58*, 11329; b) W. Yang, L. Zhang, J. Xie, X. Zhang, Q. Liu, T. Yao, S. Wei, Q. Zhang, Y. Xie, *Angew. Chem. Int. Ed.* **2016**, *55*, 6716.

[10] M. Liu, D. Jing, Z. Zhou, L. Guo, *Nat. Commun.* **2013**, *4*, 2278.

[11] P. Xia, S. Cao, B. Zhu, M. Liu, M. Shi, J. Yu, Y. Zhang, *Angew. Chem. Int. Ed.* **2020***, 59*, 5218.

[12] a) T. Di, Q. Xu, W. Ho, H. Tang, Q. Xiang, J. Yu, *ChemcatChem* **2019**, *11*, 1394-1411; b) F. Xu, J. Zhang, B. Zhu, J. Yu, J. Xu, *Appl. Catal B* **2018**, *230*, 194.

[13] a) S. Wang, Y. Gao, S. Miao, T. Liu, L. Mu, R. Li, F. Fan, C. Li, *J. Am. Chem. Soc*. **2017**, *139*, 11771−11778; b) Y. Gao, J. Zhu, H. An, P. Yan, B. Huang, R. Chen, F. Fan, C. Li, *J. Phys. Chem. Lett.* **2017**, *8*, 1419.

[14] a) K. F. Wu, W. E. Rodriguez-Cordoba, Y. Yang, T. Q. Lian, *Nano Lett*., 2013, *13*, 5255; b) T. Yoshihara, R. Katoh, A. Furube, Y. Tamaki, M. Murai, K. Hara, S. Murata, H. Arakawa, M. Tachiya, *J. Phys. Chem. B* **2004**, *108*, 3817; c) C. Ye, J. Li, Z. Li, X. Li, X. Fan, L. Zhang, B. Chen, C. Tung, L. Wu, *ACS Catal*. **2015**, *5*, 6973.

[15] F. Liu, R. Shi, Z. Wang, Y. Weng, C. Che, Y. Chen, *Angew. Chem. Int. Ed*. **2019**, *131*, 11917.

[16] R. Shi, H. Ye, F. Liang, Z. Wang, K. Li, Y. Weng, Z. Lin, W. Fu, C. Che, Y. Chen, *Adv. Mater*. **2018**, *30*, 1705941.

[17] a) C. C. Chen, W. H. Ma, J. C. Zhao, *Chem. Soc. Rev.* **2010**, *39*, 4206; b) J. Hu, D. Chen, Z. Mo, N. Li, Q. Xu, H. Li, J. He, H. Xu, J. Lu, *Angew. Chem. Int. Ed.* **2019**, *58*, 2073; c) J. H. Baek, T. M. Gill, H. Abroshan, S. Park, X. Shi, J. Nørskov, H. S. Jung, S. Siahrostami, X. Zheng, *ACS Energy Lett.* **2019**, *4*, 720.

[18] a) J. Liu, Y. Liu, N. Liu, Y. Han, X. Zhang, H. Huang, Y. Lifshitz, S. T. Lee, J. Zhong, Z. Kang, *Science,* **2015**, *27*, 970; b) S. Gao, T. Chan, Y. Lu, X. Shi, B. Fu, Z. Wu, H. Li, K. Liu, S. Alzuabi, P. Cheng, M. Liu, T. Li, X. Chen, L. Y. Piao, *Nano Energy,* **2020**, *67*, 104287; c) W. Che, H. Su, X. Zhao, Y. L. Li, H. Zhang, W. L. Zhou, M. H. Liu, W. R. Cheng, F. C. Hu, Q. H. Liu, *J. Mater. Chem. A* **2019**, *7*, 17315; d) T. Jeon, H. Kim, H.-i. Kim, W. Choi, *Energy Environ. Sci.* 2020.

[19] S. Siahrostami, G. Li, V. Viswanathan, J. K. Nørskov, *J. Phys. Chem. Lett.* **2017**, *8*, 1157.

[20] a) M. Xiao, Z. Wang, M. Q. Lyu, B. Luo, S. C. Wang, G. Liu, H. M. Cheng, L. Z. Wang, *Adv. Mater*. **2018**, *31*, 1801369; b) X. J. Wang, J. Feng, Y. C. Bai, Q. Zhang, Y. D. Yin, *Chem. Rev*. **2016**, *116***,** 10983; c) Li, W. J. Zhu, C. C. Li, T. Wang, J. L. Gong, *Chem. Soc. Rev*. **2019,** *48*, 1874; d) E. H. Zhang, J. Liu, M. W. Ji, H. Z. Wang, X. D. Wan, H. P. Rong,

W. X. Chen, J. J. Liu, M. Xu, J. T. Zhang, *J. Mater. Chem. A* **2019**, *7*, 8061; e) L. Cheng, Q. Xiang, Y. Liao, H. Zhang, *Energy Environ. Sci.* **2018**, *11*, 1362.

[21] a) X. Li, Y. Sun, J. Xu, Y. Shao, J. Wu, X. L. Xu, Y. Pan, H. Ju, J. Zhu, Y. Xie, *Nat. Energy* **2019,** *4*, 690; b) S. Wang, B. Guan, Y. Lu, X. Lou, *J. Am. Chem. Soc*. **2017**, *139*, 17305. c) B. Xu, P. He, H. Liu, P. Wang, G. Zhou, X. Wang, *Angew. Chem. Int. Ed*. **2014**, *53*, 2339.

[22] J. Liu, J. Feng, J. Gui, T. Chen, M. Xu, H. Wang, H. Dong, H. Chen, X. Li, L. Wang, Z. Chen, Z. Yang, J. Liu, W. Hao, Y. Yao, L. Gu, Y. Huang, X. Duan, J. Zhang, Y. Li, *Nano Energy* **2018**, *48*, 44.

Table of Contents

**Visually Resolving the Direct Z-Scheme Heterojunction in CdS@$ZnIn_2S_4$ Hollow Cubes for Photocatalytic Evolution of $H_2$ and $H_2O_2$ from Pure Water**

*Erhuan Zhang, Qianhong Zhu, Junheng Huang, Jia Liu,* Guoqiang Tan, Chenjun Sun, Tao Li, Shan Liu, Yuemei Li, Hongzhi Wang, Xiaodong Wan, Zhenhai Wen, Fengtao Fan and Jiatao Zhang,* Katsuhiko Ariga*

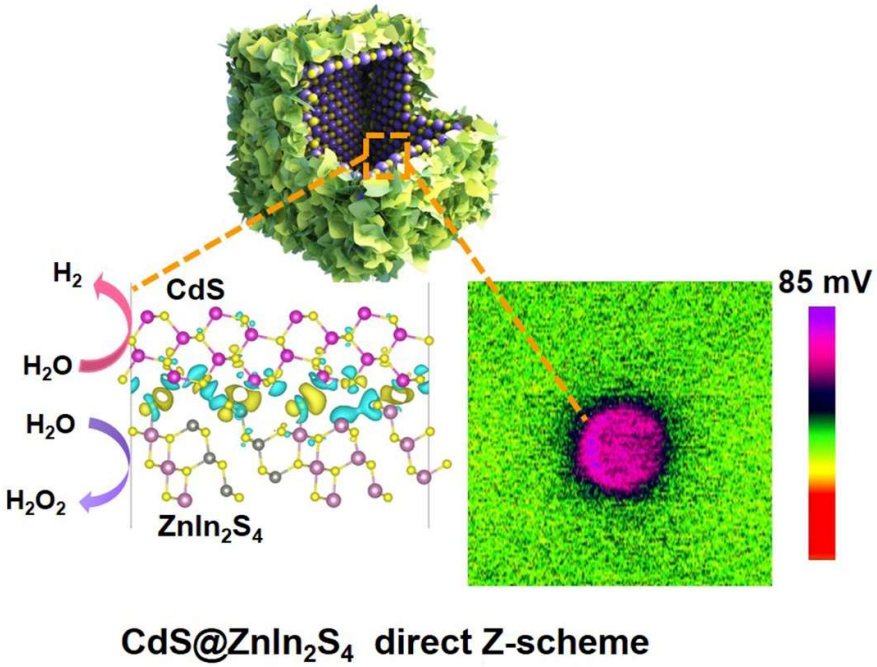


The CdS@$ZnIn_2S_4$ hollow cubes with well-defined hetero-interfaces have been fabricated, which can effectively split pure water into $H_2$ and $H_2O_2$ with a stoichiometric ratio close to 1:1 under visible light irradiation. The spatial-resolved surface photovoltage spectroscopy study has been also exploited to give the first visualized demonstration on the formation of the direct Z-scheme heterojunction of CdS@$ZnIn_2S_4$.